Solution Structure of Two New Toxins from the Venom of the Chinese Scorpion *Buthus martensi* Karsch Blockers of Potassium Channels[†,‡]

Eric Blanc,[§] Régine Romi-Lebrun,[||] Olivier Bornet,[§] Terumi Nakajima,[||] and Hervé Darbon*[,§]

AFMB, CNRS UPR 9039, IFR1, 31, Chemin Joseph-Aiguier, 13402 Marseille Cedex 20, France, and Suntory Institute for Bioorganic Research, Mishima-Gun, Shimamoto-Cho, Wakayamadai 1-1-1, Osaka 618, Japan

Received April 24, 1998; Revised Manuscript Received July 1, 1998

ABSTRACT: The solution structure of BmTX2 purified from the venom of the Chinese Buthid *Buthus martensi* has been determined by 2D NMR spectroscopy techniques which led to the description of its 3D conformation. The structure consists of a triple-stranded β-sheet connected to a helical structure. This helix encompasses 10 residues, from 11 to 20, begins with a turn of 3_{10} helix, and ends with an α helix. The three strands of β sheet comprise residues 2−6, with a bulge covering residues 4 and 5, 26−29, and 32−35, with a type I′ β turn centered on residues 30−31. We also characterized the solution structure of BmTX1. The two toxins which are potent blockers of both large-conductance calcium-activated potassium channels (BK_{Ca} channels) and voltage-gated potassium channels (Kv1.3) are highly superimposable and possess the same structural characteristics. Analysis of these structures allows us to hypothesize that, besides the main surface of interaction described by the functional map of charybdotoxin, one can expect that the binding of scorpion toxins on BK_{Ca} channels may involve residues on the edge of this surface.

Numerous toxins have now been purified from the venom of various scorpions. According to their determined activity, these toxins were divided into different classes, depending upon their respective targets. This classification is also correlated to the size of the toxins. The first major class is made of the so-called long neurotoxins which constitute a homogeneous class of proteins of 60−70 residues reticulated by four disulfide bridges and directed against sodium channels (*1, 2*). The second major class is formed by the toxins specific for potassium channels. They all are proteins of 29−39 amino acids reticulated by three disulfide bridges (*3*−*10*) or four in maurotoxin (MTX)[1] (*11*), Pi1 (*12*), and HsTX1 (*13*).

Thanks to the analysis of the binding potency of natural toxins and generated mutants, the interacting surface of scorpion toxins with potassium channels has been described (*14, 15*). Later, the receptor counterparts for some of the critical residues of the toxins were identified (*14, 16, 17*). Beyond a simple explanation of the mechanism of the blocking phenomenon, the structures of scorpion toxins directed against potassium channels were used as molecular calipers to precisely map their binding site (*18*−*21*). Therefore, different models of pore-forming regions of the voltage-gated Shaker-related potassium channels were defined (*22*−*24*). While the interaction of the scorpion toxins with the voltage-gated potassium channels is well-known, the interaction of other scorpion toxins with the large- and small-conductance calcium-activated potassium channels (BK_{Ca} and SK_{Ca} respectively) is still unclear. As far as the SK_{Ca} is concerned, this delay is the result of a delayed knowledge of the channel primary structure (*25*).

Study of the interaction of the charybdotoxin (CTX) toxin family with the BK_{Ca} channels is also less advanced than with Kv channels. We know the important residues of charybdotoxin for its binding to BK_{Ca} (*26, 27*), but we do not know the BK_{Ca} counterparts of these residues. This is partly due to the presence of an additional β subunit to the α subunit which contains the pore-forming region. The β transmembrane subunit has been recently found to directly participate in the high-affinity binding site of the charybdotoxin (*28*−*30*). Further analysis of the scorpion toxin/BK_{Ca} channel complex should take into account this new partner in the interaction. In that field, characterization of new toxins is of great interest in providing new high-affinity natural analogues.

The venom of the Chinese scorpion *Buthus martensi* Karsch was poorly characterized until recently, when the first two groups of toxins directed against potassium channels were purified and characterized. The first group is composed of four toxins, belonging to the leiurotoxin family, which are directed against SK_{Ca} channels (*31*). The second group of toxins, composed of BmTX1, BmTX2, and BmKTX, is active on the voltage-gated potassium channels, as these three toxins are able to compete with [^{125}I]KTX for the binding to rat brain synaptosomes. Two of these toxins, namely

[†] This work was supported in part by the Association Francaise contre les Myopathies.

[‡] The coordinate files have been deposited in the Brookhaven Protein Data Bank (codes 1big and 2bmt).

* To whom correspondence should be addressed. E-mail: herve@afmb.cnrs-mrs.fr. Tel: (33) 491-16-45-35. Fax: (33) 491-16-45-36.

[§] AFMB, CNRS UPR 9039.

[||] Suntory Institute for Bioorganic Research.

[1] Abbreviations: CTX, charybdotoxin; MTX, maurotoxin; KTX, kaliotoxin; AgTX2, agitoxin 2; NTX, noxiustoxin; MgTX, margatoxin; IbTX, iberiotoxin; BK_{Ca}, large-conductance calcium-activated potassium channel; SK_{Ca}, small-conductance calcium-activated potassium channel; Kv, Shaker-related voltage-gated potassium channel.

S0006-2960(98)00937-4 CCC: $15.00
Published on Web 08/20/1998

BmTX1 an BmTX2, belonging to the CTX family, are also potent blockers of the BK_{Ca} channels. BmTX1 and BmTX2 compete with [^{125}I]CTX for the binding to BK_{Ca} channels with IC_{50} of 650 and 300 pM, respectively, which has to be compared with an IC_{50} of 7.2 pM for unlabeled CTX. Thus, these two toxins present the same specificity as their group header; i.e., they are directed against BK_{Ca} channels and Kv channels, but their binding potencies are different.

In this paper, we investigate the structures of BmTX1 and BmTX2 to get new insight into their activity and/or specificity. Through this analysis, we demonstrate that the differences observed between these three toxins are not related to a modified structure but to point mutations. The functional map of BmTX2 is similar to that of charybdotoxin when the one of BmTX1 is truncated by one residue which allowed us to hypothesize that an interaction outside the CTX functional map could be involved in different binding characteristics of these toxins.

MATERIALS AND METHODS

Sample Preparation. The two toxins, BmTX1, and BmTX2 were synthesized by solid-phase synthesis, as described elsewhere (*10*). The so-obtained synthetic peptides were dissolved in 0.5 mL of H_2O/D_2O (90/10 v/v), pH 3, uncorrected for isotope effects, leading to a concentration of 2 mM. The amide proton exchange rate was determined after lyophilization and dissolution in 100% D_2O.

NMR Spectroscopy. All ^{1}H 2D NMR measurements were carried out using a Bruker DRX 500 spectrometer equipped with a HCN probe, and self-shielded triple axis gradients were used. The experiments were performed at two temperatures, 283 and 300 K, to solve assignment ambiguities. Two-dimensional spectra were acquired using the States−TPPI method (*32*) to achieve F_1 quadrature detection (*33*). The spectral width in both dimensions was 6000 Hz, and for all experiments except DQF-COSY, the data size was 2048 points for t_2 and 512 points for t_1 increments, with 64 transients per experiment. For the DQF-COSY, the data size was 4096 points for t_2 and 512 points for t_1. Water suppression was achieved using presaturation during the relaxation delay (1.5 s), and during the mixing time in the case of NOESY experiments, or using a watergate 3-9-19 pulse train (*34, 35*) using a gradient at the magic angle obtained by applying simultaneous *x*-, *y*-, and *z*-gradients prior to detection. NOESY spectra were acquired using mixing times of 80 and 120 ms. Clean TOCSY (*36, 37*) was performed with a spin-locking field strength of 8 kHz and mixing time of 80 ms. The amide proton exchange experiments were recorded immediately after dissolution of the peptides in D_2O. A series of NOESY spectra with a mixing time of 80 ms were recorded at 300 K, the first one for 1 h, followed by spectra of 10 h each.

Data Processing. Spectra were processed with NMRPipe (*38*) and Bruker's UXNMR software, running on Silicon Graphics Indy R4400. The matrices were transformed to a final size of 2048 points in the acquisition dimension and to 1024 points in the other, except for coupling constant determination for which a 8192 × 1024 matrix was used. The signal was multiplied by a shifted sine bell window in both dimensions prior to a Fourier transform, and then a fifth-order polynomial baseline correction was performed.

Spectral Analysis. The sequential assignment following the amino acid spin system identification was done using the well-known Wüthrich strategy (*39*−*42*).

Experimental Restraints. The integration of the NOE data collected was done by the line shape integration routine of the EASY software (*43*), running on a SUN-IPC workstation. Obtained volumes were then converted into distance restraints by the CALIBA routine of the DYANA software (*44*). The values of ϕ torsion angles constraints were obtained as described previously (*45*). Briefly, the $^3J_{HN\alpha}$ coupling constants were obtained using the INFIT routine of the XEASY software (*46*) and were then translated into −40°/−70° and −70°/−170° angle restraints corresponding to small (<7 Hz) and large (>8 Hz) coupling constants, respectively.

Structure Calculations. Distance geometry calculations were performed with the variable target function programs DIANA (*47*) and DYANA (*44*). As described previously (*42, 45*), a set of 1000 structures was initiated, taking into account the intraresidual and sequential distance constraints. The 500 best structures were refined using the medium-range distance constraints. Of these, only 250 structures were kept for a third round of calculation including the whole NOE derived data set and additional constraints corresponding to the three disulfide bridges. A REDAC strategy (*48*) was finally used with the 50 best structures, to include dihedral constraints and additional distances coming out from the hydrogen bonds.

The 25 structures with the lowest constraint violations and hence the lowest target function were energy minimized over 10 000 iterations of the Powell algorithm of the X-PLOR 3.84 software (*49*), using a CHARMM force field.

The visual analysis of resulting structures was carried out with the TURBO-FRODO graphic software (*50*) as well as with MOLMOL software (*51*) running on Silicon Graphics workstations. RMSD values were obtained by X-PLOR software.

RESULTS AND DISCUSSION

Sequential Assignment. The spin systems of both BmTX1 and BmTX2 were identified on the basis of both COSY and TOCSY spectra. The ambiguities due to overlapping signals were solved by the comparative use of spectra recorded at two temperatures, 283 and 300 K.

For BmTX1, the first starting position for defining the sequential assignment was the unique arginine R34. Using mainly the $H\alpha-HN_{i,i+1}$ connectivities, it has been possible to connect up to S37 and down to M29 (each assumption was confirmed by either $H\beta-HN_{i,i+1}$ or $HN-HN_{i,i+1}$ correlation peaks). Next, we used one of the two valines taken as V5. This allowed us to connect the polypeptide chain down to 1 and up to 10, by virtue of strong $H\alpha-HN_{i,i+1}$ connectivities. From residue 10, strong $HN-HN_{i,i+1}$ peaks helped us to establish the connectivities up to F21; the proline P15 was connected to both W14 and V16, respectively, by $HN-H\delta_{i,i+1}$ and $H\delta-HN_{i,i+1}$ correlation peaks. The remaining proline, assigned as P23 was then used as the last starting point to obtain the sequential assignment of segment 23−29 in BmTX1. One connection remained not observable (Figure 1), between F21 and G22, as they possess the same HN chemical shift. These amino acids were assigned

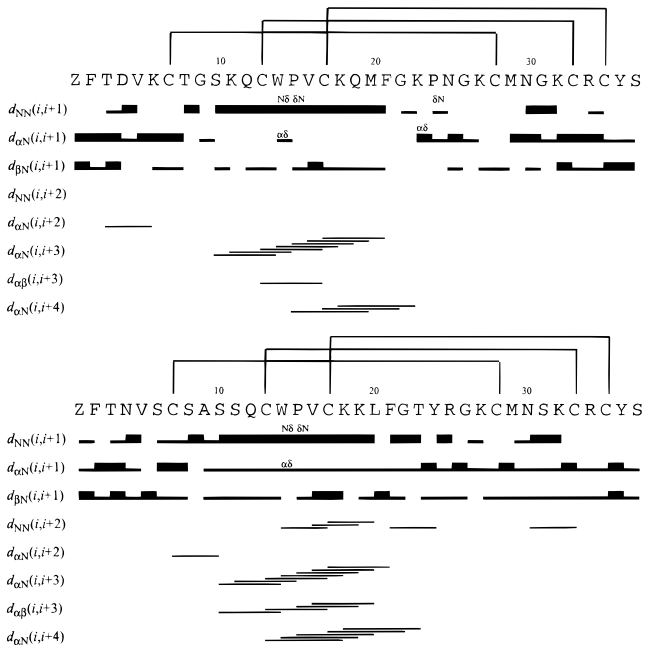

FIGURE 1: Amino acid sequence of BmTX1 (top) and BmTX2 (bottom) and a survey of NMR data used for locating the secondary structure elements: the sequential NOE's, extracted from NOESY with mixing times of 80 ms (BmTX1) or 120 ms (BmTX2) and classified as weak or strong, are represented by the thickness of the bars.

unequivocally as they were the only remaining spin systems. At the end of this procedure, nearly all proton resonances were assigned.

The sequential connectivities obtained from NOESY spectra for the BmTX2 are illustrated in Figure 1. Due to the high level of homology of BmTX2 spectra with those of the preceding toxin, the sequential assignment of this toxin was easily obtained, taking as the first starting point the unique proline to connect the segment 10−20, by virtue of strong HN−$HN_{i,i+1}$ peaks. The alanine A9 (for the N-terminal segment) and threonine T23 (for the C-terminal part) were then used to get the complete sequential assignment of BmTX2 (Figure 1 and Table S1 in Supporting Information).

Structure Determination. *(A) Hydrogen Bonds*. We measured the exchange rates of amide protons of BmTX2 with the solvent. Amide protons still present after 50 h of exchange were considered as being engaged in hydrogen bonds. Most of the slowly exchanged amide protons occurred in regular secondary structures such as HN 17, 18, 19, 20, and 21 in the helix and HN 27, 29, 32, 33, and 34 in the β-sheet. The partner of the amide proton of residue 7 was identified as being the carbonyl oxygen of residue 5 during the structure refinement.

(B) Coupling Constants. We measured 30 $^3J_{HN\alpha}$ coupling constants on NOESY maps with the infit software. The missing values correspond to the N-terminal residue, the proline 15, the glycines 22 and 26, and residues 17, 25, and 37 for which infit was unable to get unambiguous values. Of these 30 coupling constants, 24 were converted into angle restraints, the others being in the 7−8 Hz range.

Secondary Structures. Analysis of the sequential and medium-range NOE correlations together with the chemical shift index (CSI) (*52*) and coupling constant values allowed to predict the secondary structure elements. The presence of strong sequential HN−HN NOE's together with medium-range Hα−$HN_{i,i+3}$, Hα−$HN_{i,i+4}$, Hα−$H\beta_{i,i+3}$ connectivities and small $^3J_{HN\alpha}$ coupling constants suggests the presence of an helical conformation. This helix could be atypical in its first turn, as can be seen from the CSI of residues 12−14 (Figure 2), the value of the $^3J_{HN\alpha}$ coupling constant of C13 (7.5 Hz), and the absence of NOE Hα−$HN_{i,i+4}$. Strong Hα−$HN_{i,i+1}$, together with weak or absent HN−$HN_{i,i+1}$, connectivities and positive values of CSI indicate an extended conformation for segment 26−36, except for residues 30 and 31, thus representing a two-stranded β sheet with a turn composed of residues 30−31.

Table 1: Structural Statistics of the 30 Best Structures

	RMSD[a] (Å)	⟨DG⟩[b]	$\overline{DG}$[c]
backbone (C, Cα, N)	0.388	0.552	
all heavy atoms	1.037	1.488	
energies (kcal/mol)			
total		87.65 ± 5.68	95.11
bonds		7.87 ± 1.04	8.99
angles		121.20 ± 2.66	126.16
improper		1.74 ± 0.20	1.96
van der Waals		−185.66 ± 5.15	−179.60
dihedral		138.71 ± 5.38	132.54
NOE[d]		3.53 ± 0.66	4.71
dihedral restraints[d]		0.25 ± 0.06	0.34
RMSD			
bonds (Å)		0.0083	0.0085
angles (deg)		2.79	2.85
impropers (deg)		0.24	0.26

[a] The RMSD values are pairwise RMSD (right) and are calculated with respect to the mean structure (left). [b] ⟨DG⟩ are the final 30 BmTX2 structures obtained by distance geometry and energy minimization. [c] $\overline{DG}$ is the mean structure obtained by averaging the coordinates of the individual DG structures best fitted to each other. [d] The energy values for NOE and dihedral restraints are calculated with the same weighting function as geometric energies.

Structure Calculations. The distance geometry calculations were performed with a final set of 434 distance constraints that can be clustered into 160 intraresidue, 144 sequential, 55 medium-range, and 75 long-range NOE's. Additionally, 9 supplementary distance restraints came from the three disulfide bridges, 22 distance restraints derived from the 11 hydrogen bonds, and 24 angle restraints derived from the coupling constant determination. The so-obtained 50 calculated structures are in good agreement with the experimental data, as no distance violations of more than 0.36 Å and no angle violation of more than 5.6° can be seen.

These 50 structures were then energy minimized through the Powell algorithm of X-PLOR 3.84 software to suppress the unwanted nonbonded contacts. This step led to a family of 25 final structures still consistent with experimental restraints as there is no NOE violation larger than 0.10 Å and no angle violation larger than 5°. The covalent geometry is respected as indicated by the low RMSD values on the bond lengths and valence angles. The 25 structures form a unique family with a RMSD of 0.37 Å for the backbone and 1.02 Å for the all heavy atoms (Table 1).

Structure Description. The 25 structures possess the same overall fold, with a low RMSD value all along the polypeptide chain. This fold is composed of the classical CSαβ motif (*53*), i.e., an α helix connected to an antiparallel β sheet by two disulfide bridges. The structure, as described

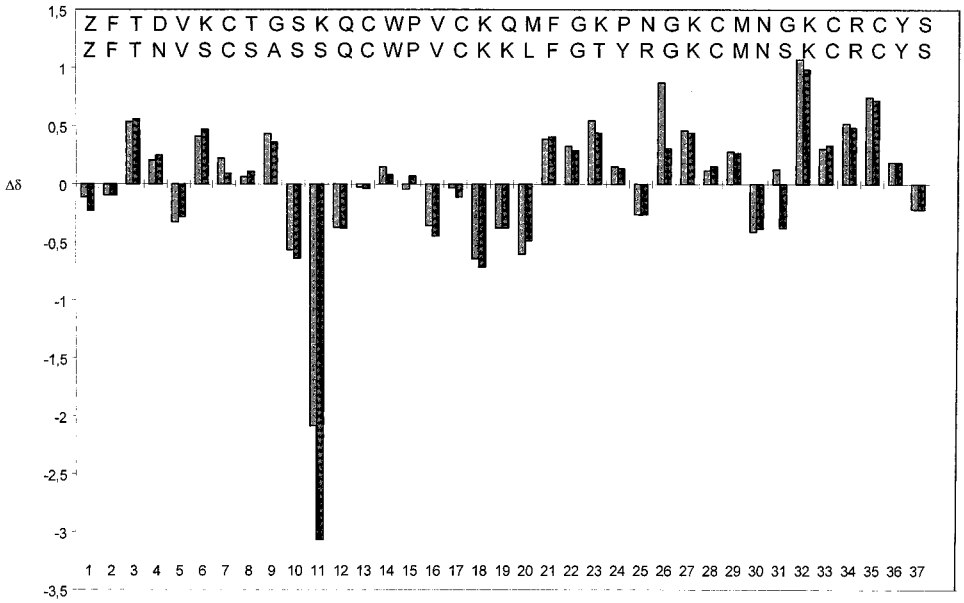

FIGURE 2: Induced shifts of the Hα protons of BmTX1 (light gray) and BmTX2 (dark gray). The amino acid sequences refer to BmTX1 (top) and BmTX2 (bottom), respectively.

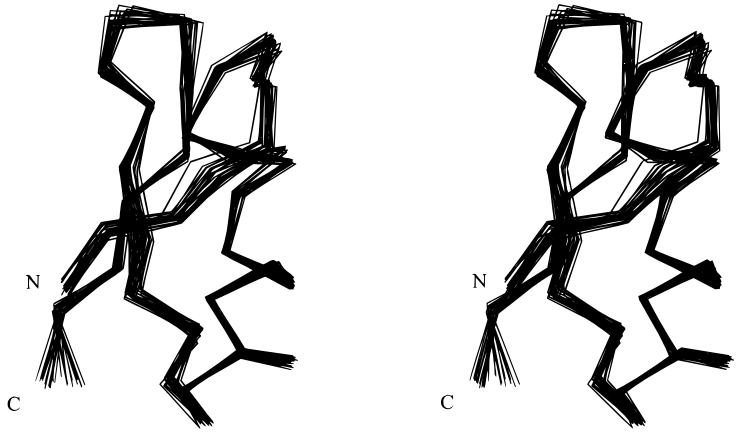

FIGURE 3: Molscript (*66*) stereoview of the 25 best molecular BmTX2 structures. Only the Cα traces are displayed.

by the MOLMOL software, is composed of a three-stranded β sheet comprising residues 2−6 (with a bulge in 4−5) for the first strand (S1) and residues 26−29 and 32−35 for the second and third one (S2 and S3), respectively. The strand S1 is separated from the S2 by a helix encompassing 10 residues from 11−20, and the S2 and S3 strands form a β hairpin (Figures 3 and 4).

The β Sheet. The two strands S2 and S3 are connected through a tight turn centered around 30−31 classified as a type I′ β turn, or turn 2.4.1 (*54*). The N-terminal segment is in a fully extended conformation and lies along the strand 32−35, stabilized by the presence of hydrogen bonds between HN 33 and O 5 on one hand and HN 7 and O 31 on the other. Despite the absence of NOE correlations characteristic for β sheet between this part and the strand S3, the segment comprising residues 2−6 is classified as the first strand of the β sheet on the basis of its overall geometry. This result is also supported by the positive values of the CSI for residues 3, 4, and 6 as well as by the values of the coupling constants of residues 3, 4, 5, and 7.

The Helix. The helix of BmTX2 is composed of two distinct parts. It starts as a 3_{10} helix (residues S11 to C13) and then continues as an α helix until residue L20. This helix is connected to the β hairpin through a αβ3 turn (*55*). Following the nomenclature of Scheerlinck et al. (*55*), the residue L1 is represented by the glycine G22 which possesses a positive ϕ angle. Then the helix should end at residue F21, and the β sheet should begin at the position R25. These two residues have ϕ/ψ couples close to that of two respective conformations.

Some distortions can be seen in the secondary structure elements. The helix is bent by the presence of a proline residue as was previously seen in other toxins such as agitoxin 2 (AgTX2) (*18*), noxiustoxin (NTX) (*56*), or MTX (*42*). The coupling constants of two of the six cysteines are unexpected. The cysteine C13 in the helix has a $^3J_{HNH\alpha}$ value higher than 6 Hz and the cysteine C33 in the β sheet has a value lower than 5 Hz (Table S1). Previous works on other toxins already described such an inconsistency. The cysteine equivalents to C13 of BmTX2 in OSK1 (*57*), CHABII (*58*), CTX (*59, 60*), NTX (*56*), margatoxin (MgTX) (*61*), and AgTX2 (*18*) have also unexpectedly high coupling constants, and low coupling constants for C33 have also been reported for Pi1 (*62*), AgTX2 (*18*), MgTX (*61*), and TsKapa (*45*). These features seem to be a characteristic of the scorpion toxin family. It can be related neither to the presence of the

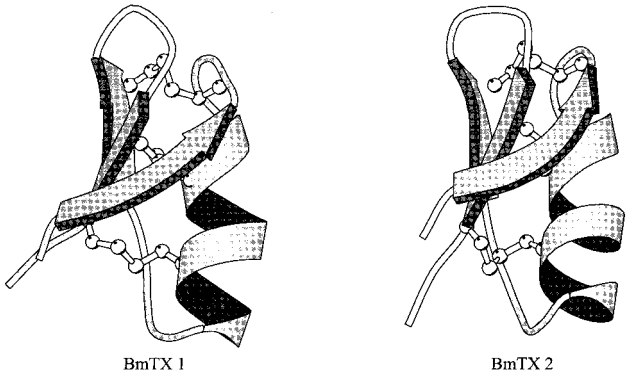

FIGURE 4: Molscript (*66*) ribbon drawing of the averaged minimized structures of BmTX1 (left) and BmTX2 (right).

disulfide bridge, as CHABII lacks this particular bridge, nor to the presence of the proline, as CTX and OSK1 lack it. This constant inconsistency is thus still mysterious.

Using a set of distances derived from a NOESY spectrum recorded with 80 ms of mixing time, we also calculated the structure of BmTX1. We thus obtained a unique family of structures, in agreement with the experimental data, composed of 199 intraresidue, 127 sequential, 30 medium-range, and 68 long-range NOE distances, distance restraints coming from 3 disulfide bridges and from 11 hydrogen bonds involving amide protons of residues 7, 16−20, 27, 29, 32, 33, 34, and 22 angular constraints derived from coupling constant measurements. The final set of 25 structures displays an overall RMSD of 0.52 Å for the backbone atoms and 1.16 Å for all heavy atoms and is of comparable energy. No NOE violations higher than 0.10 Å and angle violation higher than 5° can be seen. The structure of BmTX1 is close to that of BmTX2 (Figure 4), showing the same secondary structure elements.

As structurally related, BmTX1 and BmTX2 possess the same structural particularities; the coupling constants of C13 (7.3 for BmTX1 and 7.6 for BmTX2) and of C33 (4.3 for BmTX1 and 3.1 for BmTX2) are equivalent. Moreover, their respective Hα chemical shifts are nearly identical all along the chain, with the exception of the local differences in their primary structures (Figure 2). Even the peculiar chemical shift of the Hα of the residue S11 (1.43 ppm) shows homologies with its homologous residue in BmTX1, the Hα of the lysine 11 resonating at 2.17 ppm. The shift observed between the experimental and standard value comes from the presence of the aromatic ring of tryptophan W14. The helical conformation of this segment faces the Hα of the residue 11 to the indole ring of the tryptophan. The calculated ring current shift, following the Heigh−Mallion model implemented in MOLMOL software (*51*) is in accordance with the experimental value. Such a shift was also reported for the two other toxins possessing this tryptophan, namely CTX [Hα Lys 11 2.78 ppm (*59, 60*)] and iberiotoxin (IbTX) [Hα Lys 11 2.62 ppm (*63*)]. BmTX1 and BmTX2 are closely related and are also close to CTX and IbTX. The only visible differences between all these toxins are the orientation of the side chains, which can be assigned to the limit of the technique more than to a real difference.

BmTX1 and BmTX2 possess also some homologies with scorpion toxins belonging to the other families. The proline often observed in the α helix disturbs it, and its first turn is closer to a 3_{10} helix than to a canonical α helix as can be seen in MgTX (*61*), NTX (*56*), and AgTX2 (*18*).

Structure−Activity Relationships. We solved the structures of both BmTX1 and BmTX2 to investigate the local differences that could explain their activity and/or specificity. The Bm toxins are potent blockers of cloned voltage-gated rat brain Kv1.3 channels. BmTX1 and BmTX2 are able to inhibit the rat Kv1.3 current with IC_{50} values of 1.5 and 1.6 nM, respectively, compared with an IC_{50} of 0.7 nM for CTX (*10, 19*). Numerous works already analyzed the binding of scorpion toxins to different Shaker-related voltage-gated potassium channels. These works led to a complete description of the functional map of the CTX. The inhibition of the channel permeation is the result of a physical occlusion of the pore-forming region of the channel. The lysine K27 of the toxin is a central residue and is suspected to directly plug into the pore, coming in the vicinity of the selectivity filter. Surrounding this lysine, four other residues (N30, M29, R34, and Y36) play a key role in the interaction by directly participating to the formation of the complex. These five residues compose the functional map of the CTX on Kv channels (*14, 15*). The two Bm toxins possess the key

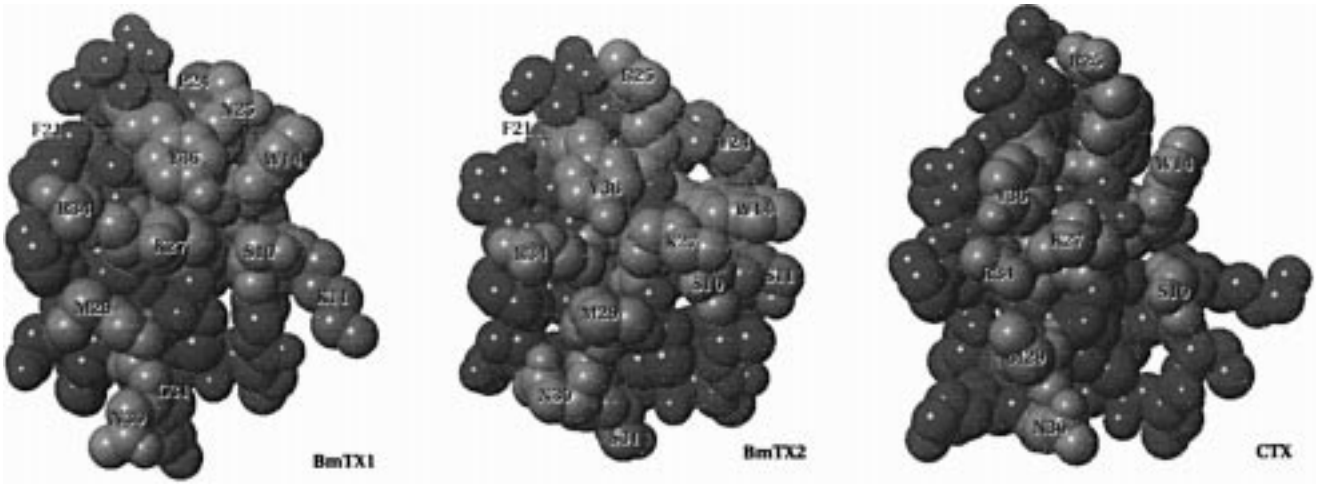

FIGURE 5: Space-filling representation of BmTX1 (left), BmTX2 (center), and CTX (right). The residues involved in the binding of CTX to the BK_{Ca} channel are colored in red. The additional residues supposed to influence the binding of both BmTX1 and BmTX2 are colored in green.

residues described for CTX. Only minor variations can be seen at the level of the side chains of some residues. Even the location of the residue 30, located in the β turn, is conserved, despite a different geometry of this turn. The conservation of the critical residues, when compared to the CTX, could explain the high affinity of these two toxins for the Kv channels.

Both BmTX1 and BmTX2 were also found to compete with [^{125}I]CTX for the binding to the BK_{Ca} channels (*10*) with IC_{50} values of 650 and 300 pM while unlabeled CTX displays an IC_{50} of 7.2 pM. As for the interaction of scorpion toxins with Kv channels, previous studies on CTX defined the functional map of CTX for the binding to BK_{Ca} channels (Figure 5). Eight residues are of first importance for the full expression of the CTX activity. The interacting surface of CTX is composed of the residues involved in the interaction with Kv channels together with three additional residues, namely S10, W14, and R25, which complete this critical surface (*26*, *27*) (Figure 5).

Analyzing the functional maps of BmTX1 and BmTX2 revealed interesting features. The BmTX2, while possessing all the previously mentioned key residues in a correct orientation, is 40 times less efficient than CTX on BK_{Ca} channels. As the backbone of these two toxins is conserved, we checked the point differences that could account for such a drop of activity. We noticed the following differences between CTX and BmTX2, i.e., respectively K11/S, K31/S, H21/F, and S24/Y. Among the residues not located on the back side (opposed to the one containing the functional map) of the toxin, only a few residues have been found to influence the binding of the toxins. The neutralization of each of the lysines K11 and K31, located on edges of CTX, results in moderate weakening in its affinity for BK_{Ca} channels as well as the substitution of the histidine 21 by a glutamine). The drop of activity noticed between BmTX2 and CTX could then be due to the addition of all these local effects. Additionally, replacing serine 24 of CTX by the bulkier side chain of the tyrosine in BmTX2 could lead to a problem of steric hindrance (Figure 5).

In BmTX1, K11 is present but K31, H21, and S24 have been replaced respectively by a glycine, a phenylalanine, and a proline. Furthermore, R25 is replaced by an asparagine, a residue which has been shown to be involved in the binding of CTX (*27*). This could well explain the difference of activity between CTX and BmTX1.

Thus we can hypothesize that, besides the main surface of interaction described by the functional map of CTX, one can expect that the binding of scorpion toxins on BK_{Ca} channels may involve residues on the edge of this surface. The recent structure determination of a potassium channel (*64*, *65*) will certainly highlight this field of research by pinpointing the spatial location of the channel residues involved in the interaction with the toxin. This can be modulated by the presence of a transmembrane β subunit in BK_{Ca} channels known to participate in the high-affinity binding site of CTX by modifying the biophysical and pharmacological properties of the α subunits (*30*).

ACKNOWLEDGMENT

We thank Jean-Guillaume Renisio for helpful discussion and Dr. Christian Cambillau for constant interest and support.

SUPPORTING INFORMATION AVAILABLE

Table S1 with chemical shifts of BmTX2 protons (2 pages). Ordering information is given on any current masthead page.

REFERENCES

1. Martin-Eauclaire, M. F., and Couraud F. (1995) in *Handbook of Neurotoxicology* (Chang, L. W., and Dyer, R. S., Eds.) pp 683−716, Marcel Dekker Inc., New York.
2. Caterall, W. A. (1980) *Annu. Rev. Pharmacol. Toxicol. 20*, 15−43.
3. Possani, L. D., Martin, B. M., and Svendsen, I. B. (1982) *Carlsberg Res. Commun. 47*, 285−289.
4. Gimenez-Gallego, G., Navia, M., Reuben, J. P., Katz, G. M., Kaczorowski, G. J., and Garcia, M. L. (1988) *Proc. Natl. Acad. Sci. U.S.A. 85*, 3329−3333.
5. Galvez, A., Gimenez-Gallego, G., Reuben, J. P., Roy-Constancin, L., Feigenbaum, P., Kaczorowski, G. J., and Garcia, M. L. (1990) *J. Biol. Chem. 265*, 11083−11090.
6. Garcia-Calvo, M., Leonard, R. J., Novick, J., Stevens, S. P., Schmalhofer, W., Kaczorowski, G. J., and Garcia, M. L. (1993) *J. Biol. Chem. 268*, 18866−18874.
7. Laraba-Djebari, F., Legros, C., Crest, M., Ceard, B., Romi, R., Mansuelle, P., Jacquet, G., Van Rietschoten, J., Gola, M., Rochat, H., Bougis, P. E., and Martin-Eauclaire, M. F. (1994) *J. Biol. Chem. 269*, 32835−32843.
8. Chicchi, G. G., Gimenez-Gallego, G., Ber, E., Garcia, M. L., Winquist, R., and Cascieri, M. (1988) *J. Biol. Chem. 263*, 10192−10197.
9. Zerrouk, H., Mansuelle, P., Benslimane, A., Rochat, H., & Martin-Eauclaire, M. F. (1993) *FEBS Lett. 320*, 189−192.
10. Romi-Lebrun, R., Lebrun, B., Martin-Eauclaire, M. F., Ishiguro, M., Escoubas, P., Wu, F. Q., Hisada, M., Pongs, O., and Nakajima, T. (1997) *Biochemistry 36*, 13473−13482.
11. Kharrat, R., Mansuelle, P., Sampieri, F., Crest, M., Martin-Eauclaire, M. F., Rochat, H., and El Ayeb, M. (1997) *FEBS Lett. 406*, 284−290.
12. Olamendi-Portugal, T., Gomez-Lagunas, F., Gurrola, G. B., and Possani, L. D. (1996) *Biochem. J. 315*, 977−981.
13. Lebrun, B., Romi-Lebrun, R., Martin-Eauclaire, M. F., Yasuda, A., Ishiguro, M., Oyama, Y., Pongs, O., Nakajima, T. (1997) *Biochem. J. 328*, 321−327.
14. Goldstein, S. A. N., Pheasant, D. J., and Miller, C. (1994) *Neuron 12*, 1377−1388.
15. Gross, A., and McKinnon, R. (1996) *Neuron 16*, 399−406.
16. Naranjo, D., and Miller, C. (1996) *Neuron 16*, 123−130.
17. Naini, A. A., and Miller, C. (1996) *Biochemistry 35*, 6181−6187.
18. Krezel, A. M., Kasibhatla, C., Hidalgo, P., MacKinnon, R., & Wagner, G. (1995) *Protein Sci. 4*, 1478−1489.
19. Aiyar, J., Withka, J. M., Rizzi, J. P., Singleton, D. H., Andrews, G. C., Lin, W., Boyd, J., Hanson, D. G., Simon, M., Dethlefs, B., Lee, C. L., Hall, J. E., Gutman, G. A., and Chandy, K. G. (1995) *Neuron 15*, 1169−1181.
20. Aiyar, J., Rizzi, J. P., Gutman, G. A., and Chandy, K. G. (1996) *J. Biol. Chem. 271*, 31013−31016.
21. Durell, S. R., & Guy, H. R. (1996) *Biochemistry 31*, 7749−7755.
22. Lipkind, G. M., and Fozzard, H. A. (1997) *J. Membr. Biol. 158*, 187−196.
23. Yang, P. K., Lee, C. Y., and Hwang, M. J. (1997) *Biophys. J. 72*, 2479−2489.
24. Kerr, I. D., and Sansom, M. S. P. (1997) *Biophys. J. 73*, 581−602.
25. Köhler, M., Hirschberg, B., Bond, C. T., Kinzie, J. M., Marrion, N. V., Maylie, J., and Adelman, J. P. (1996) *Science 273*, 1709−1714.
26. Stampe, P., Kolmakova-Partensky, L., and Miller, C. (1994) *Biochemistry 33*, 443−450.
27. Park, C. S., and Miller, C. (1992) *Biochemistry 31*, 7749−7755.

28. Hanner, M., Schmalhofer, W. A., Munujos, P., Knaus, H. G., Kaczorowski, G. J., and Garcia, M. L. (1997) *Proc. Natl. Acad. Sci. U.S.A. 94*, 2853−2858.
29. Garcia, M. L., Hanner, M., Knaus, H. G., and Kaczorowski, G. J. (1997) *Pfluegers Arch. 474*, R83.
30. Hanner, M., Vianna-Jorge, R., Kamassah, A., Schmalhofer, W. A., Knaus, H. G., Kaczorowski, G. J., and Garcia, M. L. (1998) *J. Biol. Chem. 273*, 16289−16296.
31. Romi-Lebrun, R., Martin-Eauclaire, M. F., Escoubas, P., Wu, F. Q., Lebrun, B., Hisada, M., and Nakajima, T. (1997) *Eur. J. Biochem. 245*, 457−464.
32. Marion, D., Ikuto, M., Tschudin, P., and Bax, A. (1989) *J. Magn. Reson. 85*, 393−399.
33. Marion, D., and Wüthrich, K. (1983) *Biochem. Biophys. Res. Commun. 113*, 967−974.
34. Piotto, M., Saudek, V., and Sklenar, V. (1992) *J. Biomol. NMR 2*, 661−665.
35. Sklenar, V., Piotto, M., Leppik, R., and Saudek, V. (1993) *J. Magn. Reson. 102*, 241−245.
36. Griesinger, C., Otting, G., Wüthrich, K., and Ernst, R. R. (1988) *J. Am. Chem. Soc. 110*, 7870−7872.
37. Bax, A., and Davis, D. G. (1985) *J. Magn. Reson. 65*, 355−360.
38. Delaglio, F., Grzesiek, S., Vuister, G. W., Zhu, G., Pfeifer, J., & Bax, A. (1995) *J. Biomol. NMR 6*, 277−293.
39. Wüthrich, K. (1986) in *NMR of proteins and nucleic acids*, John Wiley & Sons, New York.
40. Meunier, S., Bernassau, J. M., Sabatier, J. M., Martin-Eauclaire, M. F., Van Rietschoten, J., Cambillau, C., and Darbon, H. (1993) *Biochemistry 32*, 11969−11976.
41. Blanc, E., Fremont, V., Sizun, P., Meunier, S., Van Rietschoten, J., Thevand, A., Bernassau, J. M., and Darbon, H. (1996) *Proteins 24*, 359−369.
42. Blanc, E., Sabatier, J. M., Kharrat, R., Meunier, S., El Ayeb, M., Van Rietschoten, J., and Darbon, H. (1997) *Proteins 29*, 321−334.
43. Eccles, C., Güntert, P., Billeter, M., & Wüthrich, K. (1991) *J. Biomol. NMR 1*, 111−130.
44. Güntert, P., Mumenthaler, C., and Wüthrich, K. (1997) *J. Mol. Biol. 273*, 283−298.
45. Blanc, E., Lecomte, C., Van Rietschoten, J., Sabatier, J. M., and Darbon, H. (1997) *Proteins 29*, 359−369.
46. Szyperski, T., Güntert, P., Otting, G., & Wüthrich, K. (1992) *J. Magn. Reson. 99*, 552−560.
47. Güntert, P., Braun, W., and Wüthrich, K. (1991) *J. Mol. Biol. 217*, 517−530.
48. Güntert, P., and Wüthrich, K (1991) *J. Biomol. NMR 1*, 447−456.
49. Brünger, A. T. (1992) *X-PLOR Version 3.1 Manual*, Yale University, New Haven, CT.
50. Roussel, A., and Cambillau, C. (1989) in *Silicon Graphics Geometry Partner Directory*, pp 77−78, Silicon Graphics, Mountain View, CA.
51. Koradi, R., Billeter, M., and Wüthrich, K. (1996) *J. Mol. Graphics 14*, 51−55.
52. Wishart, D. S., Sykes, B. D., and Richards, F. M. (1992) *Biochemistry 31*, 1647−1651.
53. Cornet, B., Bonmatin, J. M., Hetru, C., Hoffmann, J. A., Ptak, M., and Vovelle, F. (1995) *Structure 3*, 435−448.
54. Oliva, B., Bates, P. A., Querol, E., Aviles, F. X., and Sternberg, M. J. E. (1997) *J. Mol. Biol. 266*, 814−830.
55. Scheerlinck, J.-P. Y., Lasters, I., Claessens, M., De Maeyer, M., Pio, F., Delhaise, P., and Wodak, S. J. (1992) *Proteins 12*, 299−313.
56. Dauplais, M., Gilquin, B., Possani, L. D., Gurrola-Briones, G., Roumestand, C., and Menez, A. (1995) *Biochemistry 34*, 16563−16573.
57. Jaravine, V. A., Nolde, D. E., Reibarkh, M. J., Korolkova, Y. V., Kozlov, S. A., Pluzhnikov, K. A., Grishin, E. V., and Arseniev, A. S. (1997) *Biochemistry 36*, 1223−1232.
58. Song, J., Gilquin, B., Jamin, N., Drakopoulou, E., Guenneugues, M., Dauplais, M., Vita, C., and Menez, A. (1997) *Biochemistry 36*, 3760−3766.
59. Bontems, F., Roumestand, C., Gilquin, B., Menez, A., and Toma, F. (1991) *Science 254*, 1521−1523.
60. Bontems, F., Gilquin, B., Roumestand, C., Menez, A., and Toma F. (1992) *Biochemistry 31*, 7756−7764.
61. Johnson, B. A., Scott, P. S., and Williamson, J. M. (1994) *Biochemistry 33*, 15061−15070.
62. Delepierre, M., Prochkina-Chalufour, A., and Possani, L. D. (1997) *Biochemistry 36*, 2649−2658.
63. Johnson, B. A., and Sugg, E. E. (1992) *Biochemistry 31*, 8151−8159.
64. Doyle, D. A., Cabral, J. M., Pfuetzner, R. A., Kuo, A., Gulbis, J. M., Cohen, S. L., Chait, B. T., and MacKinnon, R. (1998) *Science 280*, 69−77.
65. MacKinnon, R., Cohen, S. L., Kuo, A., Lee, A., and Chait, B. T. (1998) *Science 280*, 106−109.
66. Kraulis, P. J. (1991) *J. Appl. Crystallogr. 24*, 946−950.

BI9809371